ChemMedChem

Chemistry Europe
European Chemical Societies Publishing

Accepted Article

Title: FOXM1 inhibitors as potential diagnostic agents: 1st generation of a PET probe targeting FOXM1 to detect triple negative-breast cancer in vitro and in vivo

Authors: David J Perez, Seyed Amirhossein Tabatabaei Dakhili, Cody Bergman, Jennifer Dufour, Melinda Wuest, Freimut D. Juengling, Frank Wuest, and Carlos Alberto Velazquez-Martinez

To be cited as: *ChemMedChem* 10.1002/cmdc.202100279

Link to VoR: https://doi.org/10.1002/cmdc.202100279

WILEY-VCH

WILEY-VCH

FULL PAPER

FOXM1 inhibitors as potential diagnostic agents: 1st generation of a PET probe targeting FOXM1 to detect triple negative-breast cancer *in vitro* and *in vivo*

David J. Pérez, [a] [c] Seyed Amirhossein Tabatabaei Dakhili, [a] Cody Bergman, [b] Jennifer Dufour, [b] Melinda Wuest, [b] Freimut D. Juengling, [b] Frank Wuest, [b] Carlos A. Velázquez-Martínez, * [a]

[a] Dr. D. J. Pérez, Dr. S. A. Tabatabaei Dakhili, Prof. C. A. Velázquez-Martínez*
Faculty of Pharmacy and Pharmaceutical Sciences
University of Alberta
Edmonton, AB. Canada T6E 2E1.
E-mail: velazque@ualberta.ca

[b] C. Bergman, J. Dufour, Dr. M. Wuest, Prof. F. D. Juengling, Prof. F. Wuest
Department of Oncology, Faculty of Medicine and Dentistry
University of Alberta.
Edmonton, AB. Canada T6E 2E1.

[c] Dr. D. J. Pérez (Present Address)
Facultad de Medicina, Unidad de Radiofarmacia/ciclotrón
Universidad Nacional Autónoma de México, Ciudad de México
C.P. 04510, CDMX, MEXICO

Supporting information for this article is given via a link at the end of the document.

Abstract: The FOXM1 protein controls the expression of essential genes related to cancer cell cycle progression, metastasis, and chemoresistance. We hypothesize that FOXM1 inhibitors could represent a novel approach to develop ^{18}F-based radiotracers for Positron Emission Tomography (PET). Therefore, in this report we describe the first attempt to use ^{18}F-labeled FOXM1 inhibitors to detect triple-negative breast cancer (TNBC). Briefly, we replaced the original amide group in the parent drug FDI-6 for a ketone group in the novel AF-FDI molecule, to carry out an aromatic nucleophilic (^{18}F)-fluorination. AF-FDI dissociated the FOXM1-DNA complex, decreased FOXM1 levels, and inhibited cell proliferation in a TNBC cell line (MDA-MB-231). [^{18}F]AF-FDI was internalized in MDA-MB-231 cells. Cell uptake inhibition experiments showed that AF-FDI and FDI-6 significantly decreased the maximum uptake of [^{18}F]AF-FDI, suggesting specificity towards FOXM1. [^{18}F]AF-FDI reached a tumor uptake of SUV = 0.31 in MDA-MB-231 tumor-bearing mice and was metabolically stable 60 min post-injection. These results provide preliminary evidence supporting the potential role of FOXM1 to develop PET radiotracers.

Introduction

The Fork head box transcription factor (FOXM1) is an essential protein that controls the expression of proteins involved in cell replication. In normal cells, the expression level of FOXM1 is almost undetectable in quiescent or fully developed cells.[1-2] However, it has been observed that the expression of FOXM1 in a wide variety of cancer cells is significantly higher than that detected in normal cell counterparts,[3] suggesting that FOXM1 can be considered as an oncogenic and carcinogenic protein.[1-2, 4] In this regard, the FOXM1 protein has gained increasing attention in medicinal chemistry, becoming a potential drug target for cancer treatment.[1-4] Nevertheless, unlike enzymes, cell receptors, or ion channels, transcription factors such as FOXM1 do not have classical drug binding sites, which reduces the options to develop small molecule drugs capable of binding to, and inhibiting, this oncogenic protein. However, despite this challenging situation, a few experimental FOXM1 "inhibitors" have been described in the scientific literature, possessing several structural differences.[5-7] Based on that, Gormally et al. reported in 2014 a series of "forkhead domain inhibitors", or FDIs, among which the heterocyclic molecule labelled as FDI-6. This molecule was the most potent and relatively selective forkhead domain inhibitor in the series.[5]

Recently, we have carried out a series of simulations of molecular modelling dynamics and identified a possible binding site, along with key amino acid residues that could be essential for drugs to exert binding interactions at the interface of the protein and its DNA domain (DBD).[8] Furthermore, our group conducted a series of experiments aimed to validate the drug binding site mentioned above, in which we subsequently reported the chemical synthesis and FOXM1 inhibitory activity of a novel group of FDI-6

derivatives. The drug recognition process required the presence of sulfur-containing heterocycles that bind to His287 in the protein.[9]

Considering that it might be possible to use a drug binding site on the DBD of the FOXM1 protein, and that the levels of this transcription factor are significantly elevated in most (if not all) cancer cell types, we hypothesize that drug binding interactions may serve not only to inhibit its transcriptional activity but also to detect its expression in vivo, serving as biomarker. This hypothesis is supported by a recent work published by Nandi et al., in which the authors propose the use of FOXM1 as a biomarker to predict prognosis and patient response to chemotherapy.[2] In this regard, among the different types of human breast cancer, the highest levels of FOXM1 have been detected in triple negative-breast cancers (TNBC).[10-11] Thus, we chose to use a triple negative-breast cancer cell line (MDA-MB-231), as well as mice xenografts from the same cell model.

Positron Emission Tomography (PET) is one of the most widely used imaging techniques for cancer diagnosis and staging using a positron emitting radionuclide.[12] Fluorine-18 (^{18}F), with a radioactive half-life of 109.8 min, has proven to be an ideal radionuclide for PET imaging and is one of the working horses for developing PET imaging probes, as demonstrated with the glucose derivative [^{18}F]FDG, the "golden standard" PET radiotracer in oncology. Furthermore, with a positron emission decay energy providing excellent spatial resolution in imaging, and a shelf live allowing for transportation from radio–pharmacies to imaging centers, ^{18}F today is the most commonly used PET radionuclide, and thus research to develop novel ^{18}F radiotracers for PET imaging is an ongoing field.[12-13]

We hypothesize that binding interactions exerted by FOXM1 inhibitors could not only inhibit its transcriptional activity but serve as PET-based imaging probes, specifically, for ^{18}F-based imaging. Following this idea, we attempted to replace the fluorine atom present in FDI-6 for an ^{18}F atom, using copper-assisted fluorination[14-15] but were unsuccessful even after several attempts under different experimental conditions. The main reason behind the lack of reactivity towards the attempted (and failed) aromatic nucleophilic substitution on FDI-6 may be the lack of an electron-withdrawing group *para* to the fluorine atom. Consequently, and prompted by these initial results, we designed the derivative AF-FDI possessing a 4-ketone group, which unlike the amide moiety, is supposed to activate the radiolabeling with ^{18}F (Figure 1).

The design of an "activated" molecule was mainly based on the chemical structure of the lead forkhead box inhibitor-6 (FDI-6) reported by Gormally et al. in 2014.[5] In the present work, we report the first attempt to use a FOXM1 inhibitor as a PET-based imaging agent to detect TNBC. The use of a highly relevant oncoprotein involved in essentially all stages of cancer initiation, cancer progression, metastasis and chemoresistance bears a significant clinical potential, because it could form the basis for the development of a new class of theranostic agents to diagnose and treat not only TNBC but any other human cancer that overexpresses the FOXM1 transcription factor.

Herein we report the synthesis of AF-FDI, its in vitro screening as FOXM1 inhibitor, its radiolabeling with ^{18}F, its cell uptake and blocking characteristics in MDA-MB-231 cells, as well as its in vivo metabolic stability and PET imaging profile using a MDA-MB-231 tumor-bearing rodent model. These experiments constitute the first steps towards the validation of FOXM1 as a potential target for theranostic agents.

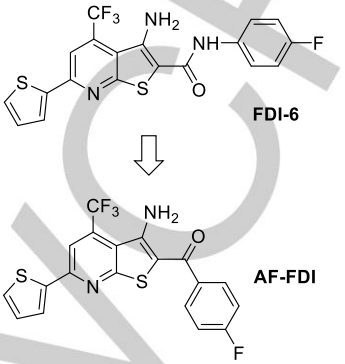

Figure 1. Chemical structures of the parent forkhead box inhibitor 6 (FDI-6) and its "activated" analogue AF-FDI possessing a 4-ketone electron withdrawing group.

Results and Discussion

Synthesis of AF-FDI.

As shown in Scheme 1, to prepare the target molecule we have modified the protocol reported for the synthesis of FDI-6 and some of its derivatives before.[5, 16-17] Briefly, the reaction between intermediates 3 and 4 under microwave irradiation yielded AF-FDI as a yellow solid in 80% yield and about 95% purity after a simple filtration from the reaction mixture (assessed by NMR, HPLC and LC-MS).

Scheme 1. Chemical synthesis of the target molecule AF-FDI.

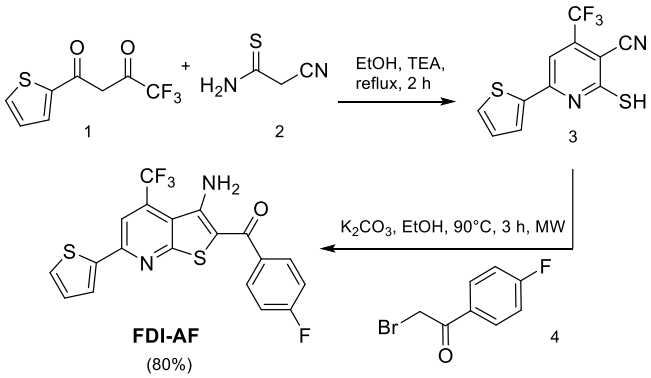

The overall yield from intermediates 1 and 2 was 80% following a two-step reaction.

Electrophoretic Mobility Shift Assay

To evaluate the binding affinity of the novel AF-FDI molecule, we determined the ability of this drug to bind to, and dissociate, the

FOXM1-DNA complex using the cell-free electrophoretic mobility shift assay (EMSA). As reported previously, this assay represents a fast and reliable way to assess direct FOXM1 inhibitory activity, and to differentiate active from inactive compounds.[5],[9] In this regard, we observed that AF-FDI exerts a direct inhibitory activity by dissociating the FOXM1-DBD with an IC_{50} = 46.38 ± 1.20 μM and Ki = 22.2 ± 0.56 μM (n = 3; Figure 2). The IC_{50} and Ki values are slightly higher, but still comparable to those determined in our lab for the parent drug FDI-6 (IC_{50} = 39.57 ± 1.15 μM; Ki = 16.8 ± 1.15 μM; n = 3).[9]

Despite the relatively high concentration of AF-FDI required to dissociate the FOXM1-DNA complex, this is in agreement with experimental results published by our group in which small-molecule FOXM1 inhibitors showed activity without affecting the levels of the SP1 transcription factor, reported to activate the expression of FOXM1 in concentrations between 30-60 μM in EMSA assay and in *vitro*.[18]

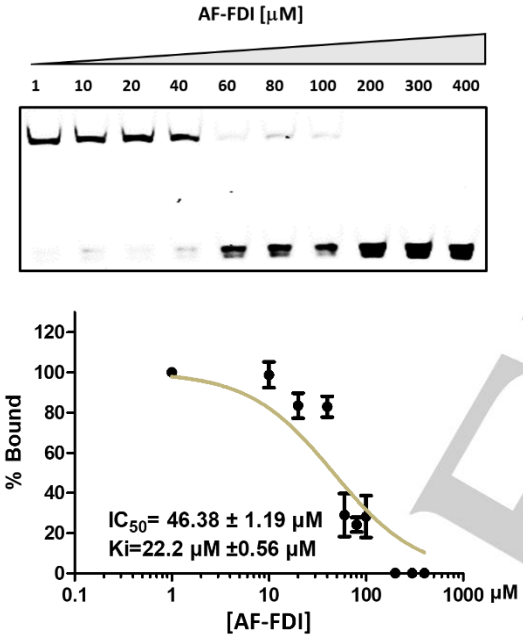

Figure 2. Electromobility shift assay (upper part) and the dose-response curve used to determine the IC_{50} and Ki values for the drug-induced dissociation of the FOXM1-DNA binding domain (lower part). Data are shown as mean + SEM calculated from 3 different experiments.

In vitro FOXM1 inhibition in MDA-MB-231 cells

After determining the binding affinity of AF-FDI, we needed to establish if this property could exert a decrease in the protein levels of FOXM1 in MDA-MB-231 cells. According to a data analysis from breast cancer patients from the Canadian Breast Cancer Foundation Tumor Bank, provided by the Cross Cancer Institute (Edmonton, AB, Canada) tissue samples obtained from patients diagnosed with breast cancer showed a 19-fold increase in FOXM1 mRNA expression compared to normal breast tissue, which was consistent with previous reports in the literature.[10] Based on the observation that FOXM1 controls its own expression,[19] we have used western blot experiments to determine the concentration-dependent effect of AF-FDI on FOXM1 protein levels. AF-FDI decreased the expression of FOXM1 in TNBC at 40, 60 and 80 μM (24 h incubation). However, the effect of AF-FDI was lower than that observed with the parent drug FDI-6 at the same test drug concentrations (Figure 3).

Test molecule AF-FDI showed a modest dose-dependent activity on inhibition of cell proliferation of MDA-MB-231 cells with an IC_{50} = 41.9 ± 1.2 μM (see Figure S5 in supporting information), which is relatively weak from a drug development standpoint, but still similar to that observed with the parent drug molecule FDI-6 (31.1 ± 8.7 μM).[9]

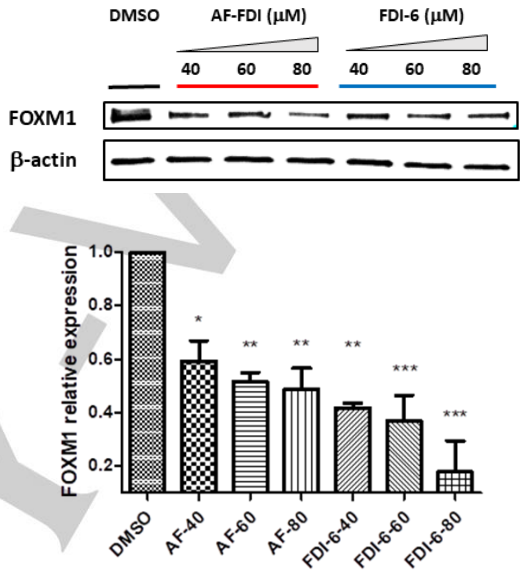

Figure 3. Concentration-dependent inhibition of FOXM1 protein levels in MDA-MB-231 triple negative-breast cancer cells. The activity of the test molecule AF-FDI was compared to that of the parent drug FDI-6 at 40, 60 and 80 μM after a 24-hour incubation period; *p < 0.05, **p < 0.01, ***p < 0.0001 compared to DMSO. Data are shown as mean + SEM calculated from 3 different experiments.

Radiochemistry

The next step involved the radiolabeling of the parent drug FDI-6 using ^{18}F to produce [^{18}F]FDI-6. We first attempted the "amide inversion" in FDI-6 to activate the ring towards the nucleophilic aromatic substitution, although we encountered chemical challenges that precluded this approach (data not shown). Then, we decided to attempt different copper-assisted fluorodeborylation reactions using the boronic ester FDI-BPin as a precursor as a path to prepare [^{18}F]FDI-6 [14-15, 20] (Scheme 2).

Scheme 2. Attempted synthesis of radiolabeled [^{18}F]FDI-6.

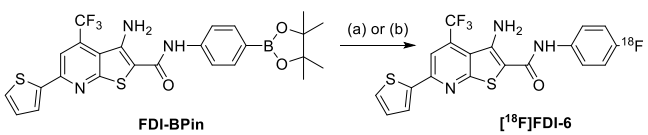

Reagents and conditions: (a) K_2CO_3, [K/K_{222}]+ $^{18}F^-$, DMF, 150˚C, $[Cu(OTf)_2(Py)_4]$; 20 min (b) Et_4NHCO_3 in n-BuOH, $^{18}F^-$, 110˚C, DMA, $[Cu(OTf)_2(Py)_4]$, 20 min. Neither of the two reaction conditions yielded the target molecule.

Nevertheless, none of the experimental conditions yielded the desired radiolabeled product (See Scheme S1 in the supporting information). We hypothesized that the presence of the unprotected amino moiety in the FDI-BPin molecule might be the cause for the lack of reactivity; in the presence of a copper catalyst the unprotected amino group may have undergone a Chan-Evan-Lan reaction side-reaction.[21-22] Prompted by these unsuccessful radiolabeling results, we considered two alternative and potentially more suitable routes to prepare the radiolabeled target molecule [^{18}F]AF-FDI. First, precursor 7 was synthesized using triflate as the leaving group during the radiolabeling nucleophilic substitution reaction by adapting a previously reported method.[23] Using this method [^{18}F]AF-FDI was obtained in 73 ± 3% radiochemical yield decay (corrected), within a 2-h time frame, a molar activity = 5.5 Gbq/μmol and a radiochemical purity (RCP) of 95% as shown in Scheme 3. After the synthesis, a log P value of 2.5 + 0.1 was determined for [^{18}F]AF-FDI, showing a moderate lipophilic profile.

Alternatively, we also prepared the precursor 9 possessing a nitro group as leaving group, yielding [^{18}F]AF-FDI in 20 ± 5% radiochemical yield, RCP = 95%, and a molar activity of 16 Gbq/μmol (See Scheme S2 in the supporting information file).

Scheme 3. Synthesis of radiolabeled [^{18}F]AF-FDI.

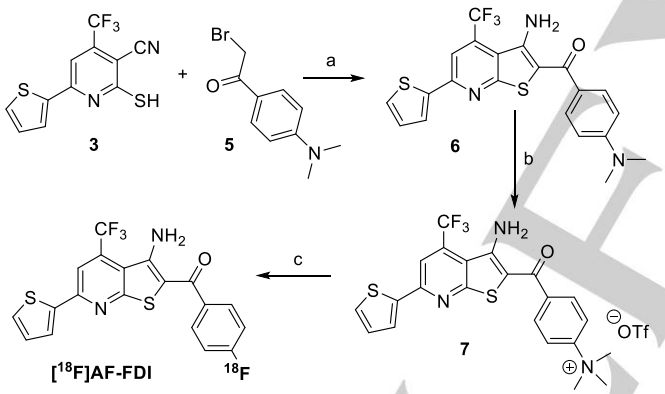

Reagents and conditions: (a) K_2CO_3, EtOH, 90˚C, 3h, MW; (b) DCM, 25˚C, $CF_3SO_3CH_3$, 18 h; (c) K_2CO_3, [K/K_{222}]+ $^{18}F^-$, 120-130˚C, CH_3CN, 15 min. The overall radiochemical yield obtained for compound[^{18}F]AF-FDI = 73 + 3%.

Cell uptake

As a next step radiolabeled [^{18}F]AF-FDI was analyzed for its in vitro profile in MDA-MB-231 cells. Uptake levels were high (~500% of radioactivity per mg of protein after 60 min incubation Figure 4A) in comparison to other experimental tracers,[20] suggesting that [^{18}F]AF-FDI is considerably taken up by TNBC cells in vitro. Furthermore, to know exactly how much of the compound would bind to the cell membrane and how much would be internalized by the cells, we also determined the percentage of the internalized fraction (cell membrane permeability). About 55% of the radiotracer was found to be internalized in MDA-MB231 cells, while ~45% seemed to be membrane-bound (Figure 4B).

Finally, to assess the specificity of [^{18}F]AF-FDI towards the target protein FOXM1, in vitro blocking experiments were performed in which cancer cells MBA-MD-231 were incubated with increasing concentrations of the non-radioactive reference compound AF-FDI, or parent compound FDI-6, before radiotracer [^{18}F]AF-FDI was added. A significant dose-dependent decrease in the maximum control cell uptake for [^{18}F]AF-FDI was observed as the concentration of AF-FDI or FDI-6 increased, reaching about 50% inhibition of the maximum cell uptake (Figure 4C). For AF-FDI an IC_{50} value of 56 μM and for FDI-6 34 μM was determined. To distinguish between compound effects and effects of percent DMSO in the inhibition solutions, control experiments with different DMSO amounts were performed as high molar stock solutions of compounds FDI-6 or AF-FDI at 1 mM contained 10% DMSO. Only the difference between inhibitory compound effects and effects of DMSO concentrations would give the real inhibition effects for FDI-6 or AF-FDI. It is also worth mentioning that the cell uptake for [^{18}F]AF-FDI could not be completely inhibited by the cold reference or FDI-6, which suggests some degree of unspecific binding (off-target binding) of the radiotracer.

Taken together, these results suggest that the novel drug AF-FDI not only has a good cell membrane permeability, but it also binds to FOXM1 inside MBA-MD-231 cells as shown by both the cell uptake and blocking experiments as well as during the western blot experiments (see Figure 3). This profile was promising for a further evaluation as a PET imaging probe.

MDA-MB-231 tumor bearing mice

[^{18}F]AF-FDI was further analyzed in vivo with a dynamic PET experiments using MDA-MB-231 tumor-bearing mice. After 60 min post injection radiotracer [^{18}F]AF-FDI reached a tumor uptake SUV_{60min} value of (0.31 ± 0.05 (n=4; Figure 5). From the dynamic PET experiments also time-activity curves (TAC) were generated for selective organ uptake and clearance profiles for [^{18}F]AF-FDI. The muscle uptake was reaching an SUV_{60min} value of 0.41 ± 0.03 (n=4; (Figure 6A) resulting in no difference between tumor and muscle uptake. It is interesting to note that the radioactivity after injection of the radiotracer in both muscle and tumor tissues was still increasing after 60 min post injection, suggesting that no equilibrium was reached yet. These observations let us conclude that [^{18}F]AF-FDI is structurally not optimized yet as it still shows non-specific behavior in vivo. However, longer observations beyond 60 min post injections as well as fine tuning of the FOXM1 inhibitor molecule structure will be necessary to generate a second-generation radiotracer targeting FOXM1 in vivo. It is worth contrasting the tumor uptake of [^{18}F]AF-FDI with that of [^{18}F]FDG (SUV_{60min} ≈ 1), reported in our previous work using the MDA-MB-231 tumor-bearing mice model, which is well validated in our lab.[24-25]

Regarding the clearance profile we observed that [^{18}F]AF-FDI is mainly cleared by the hepatobiliary path (Figure 6B), reaching its highest value at the liver right after injection, decreasing to SUV_{60min} of 8. Only a fraction of the radiotracer is cleared through the kidneys reaching a peak immediately after injection and then decreasing after a 10 min-period to a steady level from 20 to 60 min (SUV_{60min} 1.5; Figure 6C). We think that the high hepatobiliary clearance might be due to the relative lipophilic character of [^{18}F]AF-FDI (LogP = 2.58 ± 0.17), which will be considered for the design and chemical optimization of the next generation of ^{18}F-FOXM1 inhibitors. On this note, we have recently designed and published a series of troglitazone-based FOXM1 inhibitors (TFIs),[18] containing a thiazolidinedione moiety bearing an acidic

proton which, upon dissociation, should form (to some extent) a negatively charged anion at physiological pH conferring a more polar (hydrophilic) character. We hypothesize that by increasing the polarity of second generation of radiolabeled FOXM1 inhibitors, the ratio between renal and hepatobiliary clearance may improve the profile of the tracer. In this regard, we have identified one fluorine-containing lead that can be considered a scaffold to develop a 2nd generation of ^{18}F-tracers to target FOXM1 for PET imaging, which will be reported shortly.

Interestingly, we observed significant brain uptake was detected over 60 minutes suggesting that [^{18}F]AF-FDI can cross the blood brain barrier (Figure 6D), and therefore, it may be useful to reach brain tumors, opening interesting research opportunities for brain cancer.

[^{18}F]AF-FDI distributes in blood following a somewhat different profile in which the maximum drug concentration decreased immediately after the initial peak (SUV = 16) to a blood concentration that remained essentially constant from 5 to 60 minutes (SUV_{60min} = 2; Figure 6E). The comparison of blood clearance after 5 minutes with the high accumulation in the liver at the same time could also be related to the low tumor uptake since there is less tracer available in the bloodstream to reach the tumor.

Metabolism experiments

At this point it was unknown whether the radioactivity detected in the animals was due to the tissue distribution of the intact radiotracer, or the signal was detected from metabolic products resulting from a potential enzymatic degradation of [^{18}F]AF-FDI. Therefore, to assess the in vivo stability of [^{18}F]AF-FDI, metabolic stability in vivo was analyzed by administering [^{18}F]AF-FDI to normal female BALB/c mice and collecting blood samples at 5, 15, 30 and 60 min post injection. In addition, radiotracer distribution in different blood compartments was also measured. After 5 min post injection ~80% of the radiotracer was bound to red blood cells and ~20% was freely present in plasma. It is interesting to note that within 60 min, the concentration of the radiotracer detected in red blood cells oscillated ~60%, which was significant and suggests that this may be an important factor limiting the low distribution of the radiotracer towards the tumor tissue and its subsequent uptake into the tumor cells in vivo. As [^{18}F]AF-FDI is strongly bound to plasma and red cell proteins, it is possible that this might also be a contributor to the observed low tumor uptake. It merits a more detailed structural analysis to determine why the radiolabeled compound had such high affinity for red blood cells (Figure 7A). Nevertheless, by sampling the blood fractions at different time points (5, 15, 30 and 60 min) and using radio-TLC (shown in the supporting information file), after 60 min ~90% of intact [^{18}F]AF-FDI was detected, demonstrating that this molecule is relatively stable and withstands metabolic breakdown in mice (Figure 7B).

These results suggest that [^{18}F]AF-FDI is metabolically stable and therefore, suitable for longer in vivo studies in which the tissue distribution of the radiotracer can be measured at periods of time > 60 min.

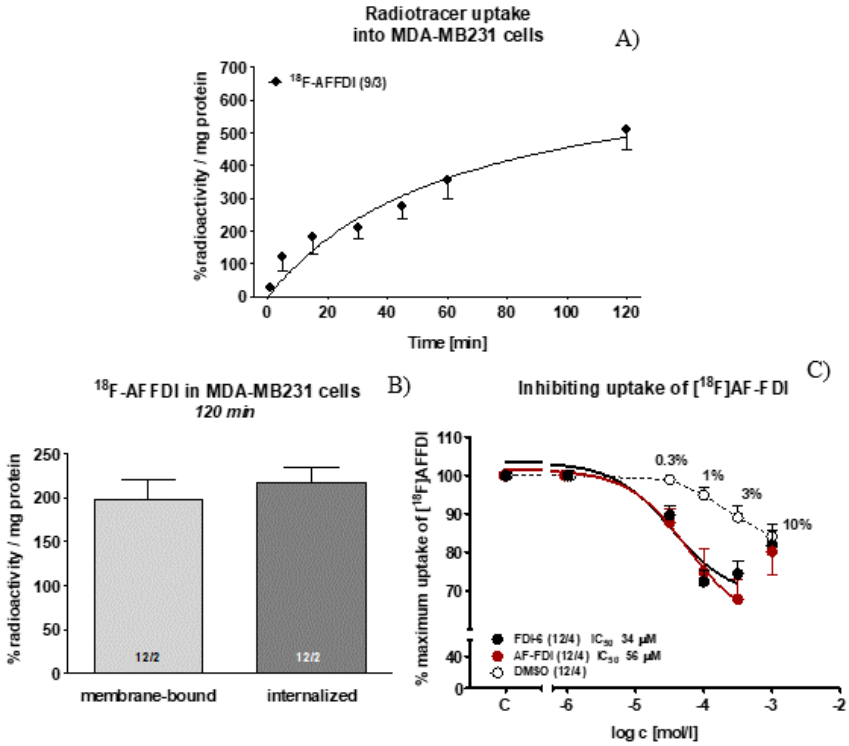

Figure 4. In vitro experiments for radiotracer [^{18}F]AF-FDI using MDA-MB-231 triple negative-breast cancer cells. A) Cell uptake; B) cell internalization, and C) uptake inhibition (blocking) using the non-radiolabeled compound FDI-AF or the parent compound FDI-6. Results are shown as mean ± SEM from n data points determined from x experiments (shown as n/x in each figure).

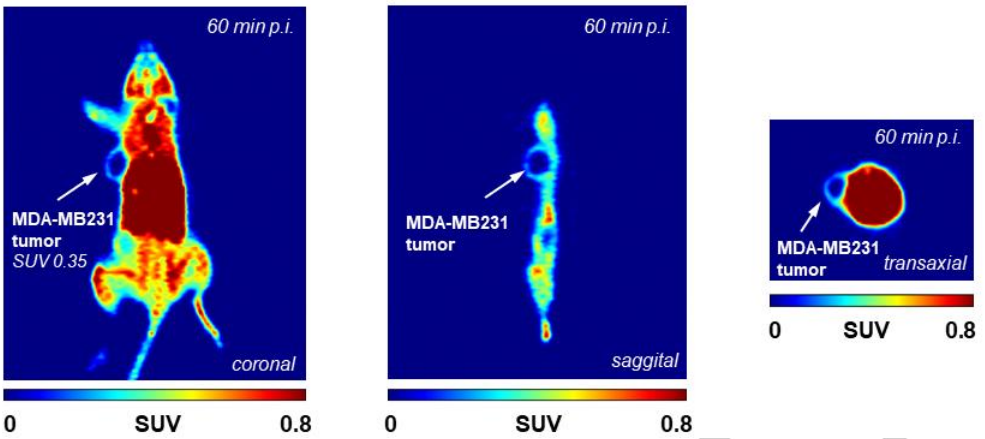

Figure 5. Representative PET images at 60 min post injection of [^{18}F]AF-FDI. From left to right: Coronal; Saggital; and Transaxial. (SUV = standardized uptake value).

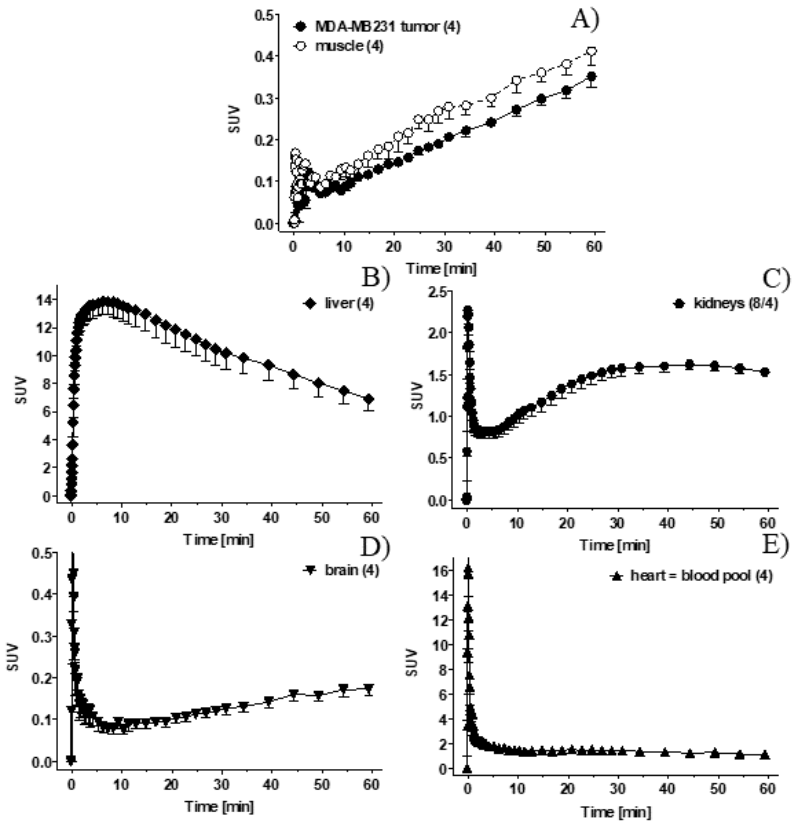

Figure 6. Time-activity curves (TACs) of the uptake and clearance profile for radiotracer [18F]AF-FDI. A) Tumor and muscle uptake; B) liver tissue clearance; C) kidney clearance; D) brain uptake; and E) blood clearance. All data are presented as mean ± SEM from n=4 experiments.

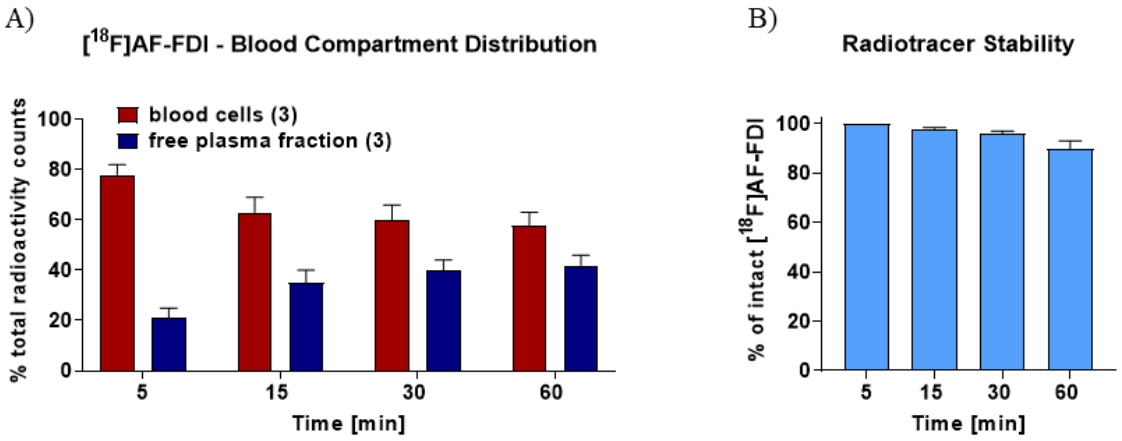

Figure 7. A) Blood compartment distribution (blood cells and free plasma fraction. B) In vivo stability of radiotracer [^{18}F]AF-FDI; in mice; the values represent mean ± SEM calculated from three experiments (n = 3).

Conclusions

In summary, to the best of our knowledge this is the first study in which the FOXM1 transcription factor is used as a potential PET imaging target to detect TNBC in vivo. The replacement of an amide group, as present in the parent drug FDI-6, for a ketone moiety in AF-FDI had only a minor effect on the activity profile of the FOXM1 inhibitor. As it was shown in the EMSA, the drug AF-FDI concentration-dependently dissociated the FOXM1-DNA complex, suggesting that the amide functionality is important but not essential. It is significant to note that during the western blot experiments some precipitation of the drug AF-FDI was observed and that this may affected the results compared to FDI-6. This observation was consistent to previous results reported by our group in which FDI-6 derivatives possessing lipophilic functional groups decreased the potency of these molecules in the western blot assay but not in the EMSA.[9]

Finally, we had circumvented the lack of reactivity toward nucleophilic aromatic substitution observed with the parent drug FDI-6, and successfully developed a nucleophilic aromatic substitution for the radiofluorination of the novel FOXM1 inhibitor AF-FDI adopted on previously reported procedures.[23] We still have to optimize the labeling conditions for future ^{18}F-labeled FOXM1 inhibitors to improve their molar activity.

The in vivo analysis of AF-FDI clearly showed that the biological profile of novel FOXM1-targeting probes will require further fine-tuning regarding optimization of tumor uptake and longer detection times beyond 60 min post injection. However, the in vivo metabolic stability of [^{18}F]AF-FDI was already superior with ~90% intact after 60 min. On the other hand, the affinity of FOXM1 targeting molecules derived from the FDI-6 structure or other scaffolds will also require further improvements for optimized structure-activity relationship to decrease its binding to blood cells and to increase the uptake into tumor cells in vivo. Also, using knock-out FOXM1 mice models, we could compare tumor uptake when FOXM1 is expressed and when not.

Experimental Section

Experimental Details.

Solvents, reagents and the building blocks: 2-thenoyltrifluoroacetone (1), 2-cyanothioacetamide (2), 2-bromo-4′-fluoroacetophenone (4), 2-bromo-1-(4-dimethylamino-phenyl)-ethanone (5). For the microwave-assisted synthesis, we used an Initiator Reactor (Biotage). All reactions were monitored by thin-layer chromatography (RediSep® TLC plates), and visualized using UV light. Melting points were measured with an electrothermal melting point apparatus (Thermofisher, USA) and were uncorrected. ^{1}H-NMR, ^{13}C-NMR and ^{19}F-NMR spectra were determined on a Bruker FT-600 MHz instrument (600, 150 and 565 MHz respectively) using DMSO-d6 as the solvent and TMS as a reference. Chemical shifts (δ) and coupling constants (*J*) are expressed in parts per million and Hertz, respectively. Signal multiplicity is expressed as *s* (singlet), *d* (doublet), *t* (triplet), *q* (quartet), *m* (multiplet) and *br* (broad singlet). Liquid Chromatography and ESI-Mass Spectrometry (LC-MS) were performed on an Agilent Technologies 1260 HPLC with C6130B MSD. The synthesis of 6-(thiophen-2-yl)-2-thioxo-4-(trifluoromethyl)-1,2-dihydropyridine-3-carbonitrile (3),[17] and FDI-6 [5, 9], was carried out following the method reported, and confirmed by ^{1}H, ^{13}C and ^{19}F NMR. Radio TLC was performed on a radio-TLC reader and Winscan analysis software. High-performance liquid chromatography (HPLC) radiochemical purifications were performed using a Phenomenex LUNA C18 column (100 Å, 250 × 10 mm, 10 mm) on a Gilson 322 pump module fitted with a 171 Diode Array and a radio detector.

Synthesis of AF-FDI and precursors 6 and 7.

We adapted the method that we reported previously for the synthesis of FDI-6 and its derivatives.[9] Briefly, a mixture of the corresponding phenone (1 equiv.), 3 (1 equiv.), and K_2CO_3 (1 equiv.) in 5mL of EtOH, was irradiated under microwave for 3 h at 90 °C in a sealed vial. After 3 h, the reaction mixture was allowed to cool down to RT to yield a precipitated that was filtered off and washed with water and hexane to yield the sought compound in an overall 70 % yield. The purity of the compound AF-FDI, and for precursors 7 and 9 used for the radiolabeling was assessed by HPLC and LC-MS.

Synthesis of [3-amino-6-(thiophen-2-yl)-4-(trifluoromethyl)thieno[2,3-b]pyridin-2-yl](4-fluorophenyl)methanone (AF-FDI).

A mixture of 4 (1 equiv., 100 mg, 0.46 mmol), 3 (1 equiv., 131 mg, 0.46 mmol) and K_2CO_3 (1 equiv., 65 mg, 0.46 mmol) in EtOH (5 mL), was irradiated under microwave for 3 h, to yield AF-FDI in a 80 % yield, as a yellowish flocculent solid; m.p. 165 °C; ^{1}H NMR (600 MHz, DMSO) δ 8.32 (s, 1H), 8.26 (dd, *J* = 3.8, 1.1 Hz, 1H), 7.91 – 7.85 (m, 3H), 7.76 (br, 2H), 7.40 (t, *J* = 8.9 Hz, 2H), 7.27 (dd, *J* = 5.0, 3.8 Hz, 1H); ^{13}C NMR (151 MHz, DMSO) δ 188.20, 164.63, 162.98, 162.79, 153.88, 148.31, 141.93, 137.00,

136.98, 133.13, 132.91, 132.09, 130.37, 130.31, 129.92, 129.22, 123.45, 121.63, 116.51, 115.73, 115.58, 112.96, 112.92, 105.07; ^{19}F NMR (565 MHz, DMSO) δ -58.53, -108.13; LCMS: found $[M+H]^+$: 423.0 m/z (calculated: 422.0 m/z for $C_{19}H_{10}F_4N_2OS_2$); Purity ≥ 95, as judged by NMR, HPLC and LC-MS.

Synthesis of [3-amino-6-(thiophen-2-yl)-4-(trifluoromethyl)thieno[2,3-b]pyridin-2-yl][4-(dimethylamino)phenyl]methanone (6).

A mixture of 5 (1 equiv., 100 mg, 0.413 mmol), 3 (1 equiv., 118 mg, 0.413 mmol) and K_2CO_3 (1 equiv., 60 mg, 0.413 mmol) in EtOH (5 mL), was irradiated under microwave for 3 h at 90 °C, to yield 6 in a 90 % yield, (172 mg, 0.38 mmol), which was used for the next step without any further purification; m.p. 245-247 °C; ^{1}H NMR (600 MHz, DMSO) δ 8.33 (*s*, 1H), 8.26 (dd, *J* = 3.8, 1.1 Hz, 1H), 7.87 (d, *J* = 1.0 Hz, 1H), 7.80 (d, *J* = 9.0 Hz, 2H), 7.51 (s, 2H), 7.28 (dd, *J* = 5.0, 3.8 Hz, 1H), 6.81 (d, *J* = 9.0 Hz, 2H), 3.05 (s, 6H); ^{13}C NMR (151 MHz, DMSO) δ 187.94, 162.27, 153.21, 152.60, 147.10, 142.11, 132.75, 132.52, 131.71, 130.05, 129.55, 129.20, 127.06, 123.57, 121.75, 117.02, 112.73, 110.86, 105.85; ^{19}F NMR (565 MHz, DMSO) δ -58.15; LCMS: found $[M+H]^+$: 448.1 m/z (calculated: 447.1 m/z for $C_{21}H_{16}F_3N_3OS_2$ %).

Synthesis of 4-{[3-amino-6-(thiophen-2-yl)-4-(trifluoromethyl)thieno[2,3-b]pyridin-2-yl]carbonyl}-N,N,N-trimethylanilinium trifluoromethanesulfonate (7).

Methyl trifluoromethanesulfonate (1.6 equiv., 72 µL, 0.63 mmol) was added dropwise to a solution of 6 (1 equiv., 172 mg, 0.38 mmol), in dry CH_2Cl_2 (5 mL) at room temperature, this mixture was stirred vigorously for 18 h to yield an orange precipitated that was filtered off and then washed with water and hexane to give precursor 7 in an 80 % yield (200 mg, 0.3 mmol), as orange flocculent crystals; m.p. > 250 °C; ^{1}H NMR (600 MHz, DMSO) δ 8.35 (s, 1H), 8.29 (dd, *J* = 3.8, 1.1 Hz, 1H), 8.16 (d, *J* = 8.9 Hz, 2H), 8.04 (d, *J* = 8.9 Hz, 2H), 7.89 (m, 1H), 7.88 (br, 1H), 7.29-7.28 (dd, *J* = 4.4 Hz, 1H), 3.68 (s, 9H); ^{13}C NMR (151 MHz, DMSO) δ 187.56, 163.01, 154.17, 148.87, 141.83, 141.70, 133.30, 133.08, 132.26, 130.15, 129.29, 129.07, 123.40, 121.75, 121.59, 121.13, 119.61, 116.35, 113.08, 104.83, 56.42; ^{19}F NMR (565 MHz, DMSO) δ -58.66, -77.76; LCMS: found: $[M+H]^+$ 462.1 m/z (calculated 462.1 m/z for $C_{22}H_{19}F_3N_3OS_2^+$); Purity ≥ 95, as judged by NMR, HPLC and LC-MS.

Electrophoretic Mobility Shift Assay (EMSA).

We employed our "in house" EMSA protocol previously reported.[9] For the protein expression and purification we used the PEX-N-GST-FOXM1-DBD plasmid (OriGene Technologies, USA) transformed into BL21(DE3) *E. Coli* cells; positive colonies were selected on LB agar plates with ampicillin (100 µg/mL). Then, these cells were grown in LB media with ampicillin (100 µg/ml) at 37 °C with orbital shaking at 220 rpm until reaching an optical density (OD600) of 0.8; protein expression was induced by adding 1 mM isopropyl β-D-1-thiogalactopyranoside (IPTG) for 6 hr at 37 °C. The GST protein and GST-FOXM1 protein from soluble fractions were purified using glutathione resin (GenScript, USA), following the manufacturer's instructions.

All values of a titration (binding) curve of recombinant FOXM1-DBD with its target double-strand DNA oligo (Forward strand: 5′-/IRD700/-AAACAAACAAACAATCAAACAAACAAACAATC-3′), were recorded using EMSA by the method previously reported by Gormally et al.[5] Briefly, dsDNA and an increasing concentration of the FOXM1 protein were incubated at RT for 30 minutes in a buffer solution containing 20 mM Tris (pH 7.5), 100 mM KCl, 1 mM EDTA, 0.1 mM DTT, and 10% glycerol, before running the samples on 6% native gel for 30 min at 120 V. The dissociation constant of protein DNA complex (Kd) was calculated using Graph pad Prism 6.2. The displacement EMSA experiments were carried out by incubating each test compound with the FOXM1 peptide, for 1.5 h, at room temperature, followed by a second incubation with DNA, for 20 minutes, before conducting the electrophoresis. The concentration of FOXM1-DBD and DNA in each reaction was 715 nM and 12.8 nM, respectively. The Ki values were calculated for each AF-FDI and FDI-6 using

Equation. 1:[26]

$$Ki = {[I]_{50}} \Big/ \left(\frac{[L]_{50}}{K_d} + {[P]_0}/{K_d} + 1\right)$$

Where: $[I]_{50}$ = IC_{50} of the inhibitor; $[L]_{50}$ = concentration of IR-labelled DNA at 50% inhibition; $[P]_0$ = concentration of the FOXM1 protein; and K_d = dissociation constant calculated from the initial titration curve.

Western blot.

We employed our reported protocol for the screening of FDI-6 and its derivatives, and used a FOXM1 mouse monoclonal antibody (Santa Cruz Biotechnology) and IRDye® 800CW Goat anti-Mouse IgM (Li-Cor Biosciences). MDA-MB-231 Cell was seeded in a density of 2 x 10^5 cells per well in 6-well plates. After treatment with AF-FDI and FDI-6 at 40, 60 and 80 µM for 24 hours, the cells were lysed with RIPA lysis and extraction buffer (Thermo Fisher) according to the manufacturer's protocol to yield the whole-cell extracts, which were then centrifuged to remove any cell debris. The protein levels in the supernatant were measured using Bradford's assay, then the protein (40 µg/lane) was loaded into a 4-20% SDS-PAGE (Sodium dodecyl sulphate polyacrylamide gel electrophoresis). After completion of the run, the protein was transferred from the gel to a nitrocellulose membrane (Thermofisher), and stained with REVERT (Li-Cor Biosciences) total protein stain, to determine total protein for normalization. Alternatively, we also used β-actin to normalize FOXM1 levels after treatment. The membrane was then detected in the 700 nm channel using Odyssey scanner (LI-COR Biosicences). The REVERT was then reversed and the membrane was blocked with 10% fat-free milk in TBST for 1 h. The membrane was incubated with the primary antibody (1:1000 dilution) at 4 °C overnight. Then, the membrane was washed three times with TBST, incubated with the corresponding Li-Cor secondary antibody and incubated again at room temperature for 1 h. The membrane was washed three times (15 minutes total) with TBST. The blots were visualized using Odyssey scanner (LI-COR Biosciences). The quantification was carried out for all proteins relative to total protein (REVERT) using ImageJ for each lane.

Radiosynthesis of [^{18}F]AF-FDI

^{18}F was produced via ^{18}O(p, n)^{18}F from $[^{18}O]H_2O$ on an ACSI TR19/9 cyclotron. [^{18}F$^-$] fluoride was trapped on a light QMA anion exchange and was eluted with Kryptofix K_{222} and K_2CO_3 in CH_3CN and dried under azeotropic conditions (nitrogen and 95 °C while adding 3 mL of CH_3CN). Compound 7 (0.0050 mmol, 2.5 mg) was dissolved in 500 µL of dry MeCN, and added to a solution of dried [^{18}F$^-$]Fluoride in 300 µL CH_3CN (typically 0.6 to 0.9 GBq). The mixture was heated to 130 °C for 15 min in a sealed vial. [^{18}F]AF-FDI was purified using HPLC (Rt= 17.5 min) linked to a radio detector (conditions: gradient CH_3CN: H_2O, starting from 80:20 ratio) and obtained in 65% decay corrected RCY, in a 95% radio purity with a molar activity 5 GBq/µmol. The octanol-water partition coefficient (LogP value) of [^{18}F]AF-FDI was measured by adapting our method previously reported method.

Cell uptake.

In vitro of cell uptake of [^{18}F]AF-FDI.

We adapted our previously reported protocol: [20, 27] MDA-MB231 cells were grown in 12-wellthe medium was removed 1 h before the experiment, cells were washed 2X with PBS and starved of glucose in glucose-free Krebs-Ringer solution (120mM NaCl, 4mM KCl, 1.2 mM KH_2PO_4, 2.5 mM

$MgSO_4$, 25 mM $NaHCO_3$, 70mM $CaCl_2$, pH = 7.4) for 1 h at 37°C. Next, 300 ml of Krebs-Ringer solution with 0.7 – 1 [^{18}F]AF-FDI was added to each well. Plates were incubated at 37°C for specific time points (5, 10, 15, 30, 60, 120 min). Radiotracer uptake was stopped with 1ml ice-cold PBS, and cells were washed 2x with PBS and lysed in 0.4 ml lysis buffer (50 mM Tris, 150 mM NaCl, 0.1% SDS, 0.5% sodium deoxycholate, 0.5%TritonX). Radioactivity in cell lysates was measured using Wizard2 Automatic g Counter (PerkinElmer; Waltham, MA, USA). Total protein concentration in the samples was determined using a Pierce Bicinchoninic Acid–Based Protein Assay (ThermoFisher Scientific). Data were calculated as the percentage of total added radioactivity per milligram of protein.

Cell internalization experiments.

Based on previously reported protocols,[20, 27] MDA-MB-231 cells were seeded 12-well plates 24–48 h before the assay so that cells could reach 95 % confluency. The medium was removed 1 h before the assay, and the cells were rinsed twice with PBS. After the addition of Krebs buffer (1 mL) to each well, the cells were incubated at 37 °C. Krebs buffer was aspirated, and the cells were incubated with 300 µL of [^{18}F]AF-FDI in 0.9 % NaCl (0.1 MBq) for 60 min at 37 °C. Cellular uptake was stopped by removing incubation media from the cells and washing the wells twice with ice-cold PBS buffer (1 mL). Surface bound radioactivity was removed from the cells by incubating the cells twice with 0.5 mL glycine-HCl in PBS (50 mM, pH 2.5) for 5 min at 37 °C. Cells were washed again with ice-cold PBS before the addition of radio-immunoprecipitation assay (RIPA) buffer (400 µL) to lyse the cells. Cells were returned into the incubator for 10 min, and cell lysates were collected for counting. Radioactivity of surface-bound and internalized fraction was measured in a WIZARD2 Automatic gamma counter (Perkin Elmer, Waltham, MA, USA). Total protein concentration in the samples was determined by the bicinchoninic acid method (BCA; Pierce, Thermo Scientific 23227) using bovine serum albumin (800, 600, 400, 300, 200, 100, 50 µg/mL, blank) as the protein standard. Data are expressed as percent of total uptake per 1 mg protein (% of total uptake/mg protein).

In vitro inhibition of [^{18}F]AF-FDI cell uptake.

According to previously reported procedures,[20, 27] the medium was removed 1 h before the experiment, and cells were washed 2X with PBS or sodium-free choline buffer (120 mM $C_5H_{14}ClNO$, 4 mM KCl, 1.2 mM KH_2PO_4, 2.5 mM $MgSO_4$, 25 mM $C5H_{14}NOHCO_3$, 70mM CaCl2, pH 7.4) and starved of glucose in glucose-free Krebs-Ringer solution. MDA-MB231 cells were incubated with Krebs-Ringer buffer or choline buffer containing [^{18}F]AF-FDI and increasing concentrations (1, 10, 100 nM and 1, 3, 7, 10mM) of reference FOXM1 inhibitor FDI-6 and non-radioactive AF-FDI. Control for 100% uptake was determined with Krebs-Ringer buffer only. After 60 min, cells were rinsed with ice-cold PBS or ice-cold choline buffer, lysed, and counted for radioactivity as previously described.

MDA-MB-231 tumor-bearing mice.

All animal experiments were carried out as previously reported,[20, 27] following guidelines of the Canadian Council on Animal Care and were approved by the local animal care committee of the Cross Cancer Institute under protocol number AC17231. Human TNBC MDA-MB231 cells (5 3 106 cells in 100 ml PBS) were injected subcutaneously and tumors were grown for 3–4wk, reaching sizes of 200–400mm^3, resulting in 300–500-mm^3-sized tumors after 2–3 week. MDA-MB231 tumor-bearing NIH-III nude mice (Charles River) were anesthetized with isoflurane (40% O_2 60% N_2), and their body temperatures were kept constant at 37°C. Mice were positioned and immobilized in a prone position into the center of the field of view of an Inveon PET Scanner (Siemens,Munich, Germany), A transmission scan for attenuation correction was not acquired. Radioactivity present in the injection solution (0.5-ml syringe) was determined using a dose calibrator (AtomlabTM 300; Biodex Medical Systems, New York, NY, USA). After the emission scan was started, radioactivity (4–8MBq of [^{18}F]AF-FDI in 100–150 ml saline) was injected intravenously with a delay of ~15 s through a tail vein catheter. Dynamic PET data acquisition was performed in a 3-dimensional list mode for 60 min. Dynamic list mode data were sorted into sonograms with 54 time frames (10 × 2, 8 × 5, 6 × 10, 6 × 20, 8 × 60, 120,5 × 300 s).
Frames were reconstructed using Ordered Subset Expectation Maximization or maximum *a posteriori* reconstruction modes. No correction for partial volume effects was performed. Image files were further processed using the Rover v.2.0.51 software (ABX). Masks defining 3-dimensional regions of interest were set and defined by 50% thresholding. Mean standardized uptake values [SUVmean = (activity/ml tissue)/(injected activity/body weight)] (ml/kg), were calculated for each region of interest. Time-activity curves (TACs) were generated from the dynamic scans.

Metabolism experiments.

As previously reported,[20] the radiotracer solution containing ~30 MBq [^{18}F]AF-FDI in ~7% EtOH/saline was injected intravenously into normal female BALB/c mice under isoflurane anesthesia. Blood samples from the tail vein (20-40 µL) were collected at 5, 15, 30 and 60 min p.i.. Plasma was separated by centrifugation (5 min, 13,000×g) followed by plasma protein precipitation using methanol (two parts per one part plasma) and a second centrifugation step (5 min, 13,000×g). Supernatants were analyzed by radio thin-layer chromatography (radio-TLC) and radioactivity was determined using a WIZARD2 Automatic gamma counter (Perkin Elmer; Waltham, MA, USA). TLCs were developed in hexane:ethyl acetate (80:20) and analyzed using a BAS-5000 reader. [^{18}F]AF-FDI had an R_f value of 0.5-0.0 in this solvent system.

Statistical Analysis.

All in vitro data and semi quantified PET data are expressed as means (n=6) ± SEM. Graphs, time-activity curves (TAC), dose-response curves and IC_{50} were constructed and calculated using GraphPad Prism 4.0. One way ANOVA was used to analyze the data from the *in vitro* screening and was considered significant when $P < 0.05$.

Acknowledgements

D. J. P. is grateful for the Postdoctoral Fellowship (287012), granted by the National Council for Science and Technology, (CONACYT, México). The authors thank Floyd Baker, David Clendening, and Blake Lazurko, from the Edmonton Radiopharmaceutical Center for ^{18}F production on the biomedical cyclotron. The authors are also grateful to Dan McGinn (Vivarium of the Cross Cancer Institute, Edmonton, AB, Canada) for supporting the animal work. The authors also gratefully acknowledge the Dianne and Irving Kipnes Foundation for supporting the PET imaging work.

Keywords: Positron Emission Tomography, PET, diagnostic agents, breast cancer, transcription factor.

[1] C.-Y. Koo, K. W. Muir, E. W. F. Lam, *Biochim. Biophys. Acta, Gene Regul. Mech.* **2012**, *1819*, 28.
[2] D. Nandi, P. S. Cheema, N. Jaiswal, A. Nag, *Semin. Cancer Biol.* **2018**, *52*, 74.
[3] A. L. Gartel, *Expert Opin. Invest. Drugs* **2010**, *19*, 235.
[4] A. L. Gartel, *Cancer Biol. Ther.* **2015**, *16*, 185.
[5] M. V. Gormally, T. S. Dexheimer, G. Marsico, D. A. Sanders, C. Lowe, D. Matak-Vinković, S. Michael, A. Jadhav, G. Rai, D. J. Maloney, A. Simeonov, S. Balasubramanian, *Nat. Commun.* **2014**, *5*, 5165.
[6] M. Halasi, B. Hitchinson, B. N. Shah, R. Váraljai, I. Khan, E. V. Benevolenskaya, V. Gaponenko, J. L. Arbiser, A. L. Gartel, *Cell Death Dis.* **2018**, *9*, 84.

[7] L. Sun, X. Ren, I.-C. Wang, A. Pradhan, Y. Zhang, H. M. Flood, B. Han, J. A. Whitsett, T. V. Kalin, V. V. Kalinichenko, *Sci. Signaling* **2017**, *10*, eaai8583.
[8] S. A. Tabatabaei-Dakhili, R. Aguayo-Ortiz, L. Domínguez, C. A. Velázquez-Martínez, *J. Mol. Graphics Modell.* **2018**, *80*, 197.
[9] S. A. Tabatabaei Dakhili, D. J. Pérez, K. Gopal, S. Y. Tabatabaei Dakhili, J. R. Ussher, C. A. Velázquez-Martínez, *Bioorg. Chem.* **2019**, *93*, 103269.
[10] T. Yanli, W. Qixue, X. Yingbin, Q. Xiaoxia, Z. Shun, W. Yanan, Y. Yongbin, Z. Bo, *Int. J. Oncol.* **2019**, *54*, 87.
[11] R. Saba, A. Alsayed, J. P. Zacny, A. Z. Dudek, *Int. J. Breast Cancer* **2016**, *2016*, 8.
[12] O. Jacobson, D. O. Kiesewetter, X. Chen, *Bioconjug. Chem.* **2015**, *26*, 1.
[13] P. Laverman, W. J. McBride, R. M. Sharkey, A. Eek, L. Joosten, W. J. G. Oyen, D. M. Goldenberg, O. C. Boerman, *J. Nucl. Med.* **2010**, *51*, 454.
[14] M. Tredwell, S. M. Preshlock, N. J. Taylor, S. Gruber, M. Huiban, J. Passchier, J. Mercier, C. Génicot, V. Gouverneur, *Angew. Chem., Int. Ed. Engl.* **2014**, *53*, 7751.
[15] J. Zischler, N. Kolks, D. Modemann, B. Neumaier, B. D. Zlatopolskiy, *Chem. - Eur. J.* **2017**, *23*, 3251.
[16] M. I. Abdel-Monem, O. S. Mohamed, E. A. Bakhite, *Pharmazie* **2001**, *56*, 41.
[17] Y. Kawazoe, H. Shimogawa, A. Sato, M. Uesugi, *Angew. Chem., Int. Ed. Engl.* **2011**, *50*, 5478.
[18] S. A. Tabatabaei Dakhili, D. J. Pérez, K. Gopal, M. Haque, J. R. Ussher, K. Kashfi, C. A. Velázquez-Martínez, *Eur. J. Med. Chem.* **2021**, *209*, 112902.
[19] O. Tietz, S. K. Sharma, J. Kaur, J. Way, A. Marshall, M. Wuest, F. Wuest, *Org. Biomol. Chem.* **2013**, *11*, 8052.
[20] M. Litchfield, M. Wuest, D. Glubrecht, F. Wuest, *Mol. Pharmaceutics* **2020**, *17*, 251.
[21] J. C. Vantourout, R. P. Law, A. Isidro-Llobet, S. J. Atkinson, A. J. B. Watson, *J. Org. Chem.* **2016**, *81*, 3942.
[22] S. Sueki, Y. Kuninobu, *Org. Lett.* **2013**, *15*, 1544.
[23] T. Kniess, M. Laube, R. Bergmann, F. Sehn, F. Graf, J. Steinbach, F. Wuest, J. Pietzsch, *Bioorg. Med. Chem.* **2012**, *20*, 3410.
[24] I. Hamann, D. Krys, D. Glubrecht, V. Bouvet, A. Marshall, L. Vos, J. R. Mackey, M. Wuest, F. Wuest, *FASEB J.* **2018**, *32*, 5104.
[25] S. J. Mattingly, M. Wuest, E. J. Fine, R. Schirrmacher, F. Wuest, *RSC Med. Chem.* **2020**, *11*, 297.
[26] Z. Nikolovska-Coleska, R. Wang, X. Fang, H. Pan, Y. Tomita, P. Li, P. P. Roller, K. Krajewski, N. G. Saito, J. A. Stuckey, S. Wang, *Anal. Biochem.* **2004**, *332*, 261.
[27] D. Krys, I. Hamann, M. Wuest, F. Wuest, *FASEB J.* **2019**, *33*, 13837.

10.1002/cmdc.202100279

WILEY-VCH

FULL PAPER

Entry for the Table of Contents

Insert graphic for Table of Contents here.

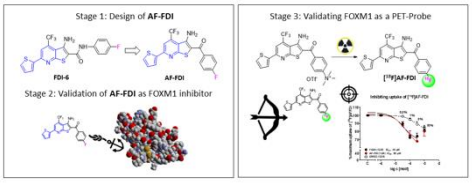

Targeting FOXM1 for triple-negative breast cancer detection. We report preliminary results to validate FOXM1 transcription factor as a target for triple-negative breast cancer detection, using a 1st generation ^{18}F-radiolabeled FOXM1 inhibitor as a PET tracer *in vitro* and *in vivo*.